the "vibration" approach to stability, where one seeks those values of compressive loads for which the frequency vanishes.[2] Thus if τ_{xx}^0 and τ_{yy}^0 (or t_{x0} and t_{y0}) are taken as positive in compression, one obtains from Eq. (9) the result that

$$\left(\frac{\tau_{xx}^0}{C_{11}}\right)_{\text{crit}} \lambda^2 + \left(\frac{\tau_{yy}^0}{C_{11}}\right)_{\text{crit}} n^2 = \frac{(\beta - \alpha^2)\lambda^4}{\lambda^4 + [(\beta - \alpha^2)/\gamma - 2\alpha]\lambda^2 n^2 + \beta n^4} + \frac{1}{12}\left(\frac{h}{R}\right)^2 [\lambda^4 + (2\alpha + 4\gamma)\lambda^2 n^2 + \beta n^4] \quad (11)$$

From Eq. (11) the critical loads for simple axial compression ($\tau_{yy}^0 = 0$), simple radial pressure ($\tau_{xx}^0 = 0, \tau_{yy}^0 = pR/h$) and hydrostatic pressure ($\tau_{xx}^0 = 1/2\tau_{yy}^0 = pR/2h$) are obtained by appropriate minimization with respect to λ and n. An interesting algorithm for accomplishing this task has recently been given by Pappas and Amba-Rao.[3]

Results

The results obtained by evaluating the lowest eigenvalue of the matrix Eq. (7) and the approximate radial frequency of Eq. (9) are displayed in Figs. 1–2. One thing that is clear immediately is the very good agreement between these two solutions, excepting only the case of a thick shell ($h/R = 1/10$) where the validity of a thin shell theory may be questionable, and in the range of $n = 2$ where the Donnell-type shell theories may not be entirely accurate.

Comparison of Figs. 1 and 2 indicates the effects of internal pressurization. One result is that the pressures drive up the frequency for a given geometry and wave number. This driving effect appears to be larger, for a given internal pressure, on the thinner shells. Another result of the pressurization is that the membrane frequencies no longer vanish as $n \to \infty$.

Similar calculations were carried out with a sharp reduction in the circumferential stiffness, in fact a drop of 80% in that stiffness. The qualitative results just indicated hold for the orthotropic shell also, except that for large wave numbers the pressurization effect makes the variation of the elastic constants negligible. In the absence of pressurization, or for small wave numbers in the presence of pressurization, the drop in the circumferential stiffness yields a sizable decrease in the frequencies of free vibration.

In other results not displayed for the sake of brevity, it is also found that the frequencies of the inplane modes of vibration are virtually insensitive to changes in the thickness-to-radius ratio of the shell for reasonably thin shells ($h/R \leq 1/20$].

Conclusions

The principal conclusions are as follows: 1) the deletion of the inplane inertia terms allows in most cases of bending of orthotropic shells a very good approximation of the "radial" frequency; 2) the change of circumferential stiffness yields sizable changes in the free vibration frequency of the radial mode; and 3) the introduction of pressurization can increase the shell's radial frequency substantially, and can eliminate entirely changes due to a decrease in the circumferential stiffness.

References

[1] Dym, C. L., "Vibrations of Pressurized Orthotropic Cylindrical Membranes," *AIAA Journal*, Vol. 8, No. 4, April 1970, pp. 693–699.

[2] Ziegler, H., *Principles of Structural Stability*, Blaisdell, Waltham, Mass., 1968, pp. 12–14.

[3] Pappas, M., and C. L. Amba-Rao, "A Discrete Search Procedure for the Minimization of Stiffened Cylindrical Shell Stability Equations," *AIAA Journal*, Vol. 8, No. 11, Nov. 1970, pp. 2093–2094.

Effect of Angle of Attack on Boundary-Layer Transition at Mach 21

MICHAEL C. FISCHER* AND DAVID H. RUDY*
NASA Langley Research Center, Hampton, Va.

Nomenclature

M	=	Mach number
$\dot{q}$	=	convective heat-transfer rate, w/m^2
R	=	Reynolds number
r_n	=	nose radius, cm
$T_{t,\infty}$	=	total temperature, °K
T_w	=	wall temperature, °K
X	=	distance along cone surface from tip, cm
θ_c	=	cone half-angle, deg

Subscripts

e	=	cone boundary-layer edge conditions at $\alpha = 0°$
E,tr	=	end of transition
S,tr	=	start of transition
∞	=	freestream conditions

FOR Mach numbers less than 11, the investigations of Refs. 1–5 indicate that angle of attack promotes sharp cone boundary-layer transition on the leeward ray while retarding transition on the windward ray. This behavior is usually attributed to the instability of the crossflow from the windward to the leeward side. However, the investigation of Ref. 6 with $M_\infty \approx 20$ and $M_e(\alpha = 0°) \approx 16$ indicated a trend opposite to this. That is, transition was retarded on the leeward ray and promoted on the windward ray. This conflicting behavior was attributed to the large local Mach number changes caused by angle of attack and the subsequent effect of this local Mach number change on transition. The present investigation is intended to reassess the results of Ref. 6 and extend the transition data over a wider angle-of-attack range utilizing alternate instrumentation. Testing occurred in the same facility as for the previous investigation[6] and employed a cone of identical external geometry.

The model used in the present investigation was a 152.4 cm long, 2.87° half-angle smooth cone, fabricated from 347 stainless steel and instrumented with thermocouples and pressure orifices. Skin thickness at the thermocouple location was 0.015 cm and nose radius 0.010 cm. The data were obtained in the Langley 22-in. Mach 20 helium tunnel which has an axisymmetric contoured nozzle. Angle of attack was in the range $\alpha = 0°$–3° with the freestream Reynolds number maintained at about 0.47×10^6/cm. All tests were conducted in unheated flow ($T_{t,\infty} \approx 300$°K) with $T_w/T_{t,\infty} \approx 1.0$ and a freestream Mach number of 21.5.

Typical heat-transfer distributions on the cone surface are presented in Fig. 1 for $\alpha = 0°$ and $\alpha = 1°$. Since these tests were conducted at $T_w/T_{t,\infty} \approx 1.0$, the heat flux was from the model to the flow ($-\dot{q}$). The boundary-layer transition location was taken as the location where the heat-transfer data first departed from the laminar level. The results of the present transition measurements, shown in Fig. 2, along with the results of Ref. 6, indicate that transition generally moves forward on the leeward ray with little movement on the windward ray, except for $\alpha = 0°$–1° where an apparent reversal takes place on both rays. This result is in direct conflict with the findings of Ref. 6. Since both investigations were conducted in the same facility and both models had the same external geometry with nearly identical nose radii the discrepancy in results is attributed to the different methods of transition detection. Additional tests were conducted using a 0.0025-cm nose radius tip with no measurable change occurring

Received January 25, 1971.

* Aerospace Engineer, Viscous Flow Section, Hypersonic Vehicles Division.

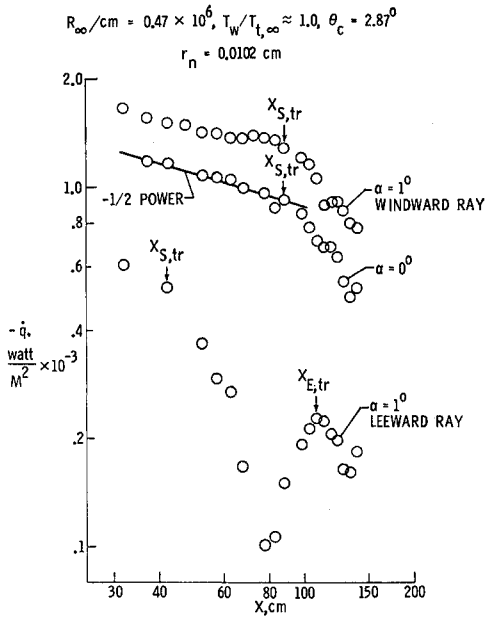

Fig. 1 Typical heat-transfer distributions on the cone surface.

in the transition location as compared to results using the 0.010-cm nose radius tip so that the slight difference in nose radii between the present tests and that of Ref. 6 is not believed to have influenced the results. In Ref. 6, a surface Pitot probe was positioned at a fixed location, 5.08 cm from the cone base, and the tunnel total pressure level was varied. The point where the surface Pitot reading began to rise from some established level was taken as the location of transition. By varying the tunnel total pressure (unit Reynold number) level both the acoustic radiated pressure intensity and model boundary-layer thickness changed and therefore the results of Ref. 6 may not be a true indication of angle-of-attack effects on transition.

The angle-of-attack transition behavior on the leeward ray of the present investigation exhibits a similar forward movement trend as compared with lower hypersonic Mach number data[1–5,7] except for the apparent transition reversal for $\alpha < 1°$ which has never been reported. This apparent transition reversal behavior which occurs on both the windward and leeward rays may result from a combination of two effects;

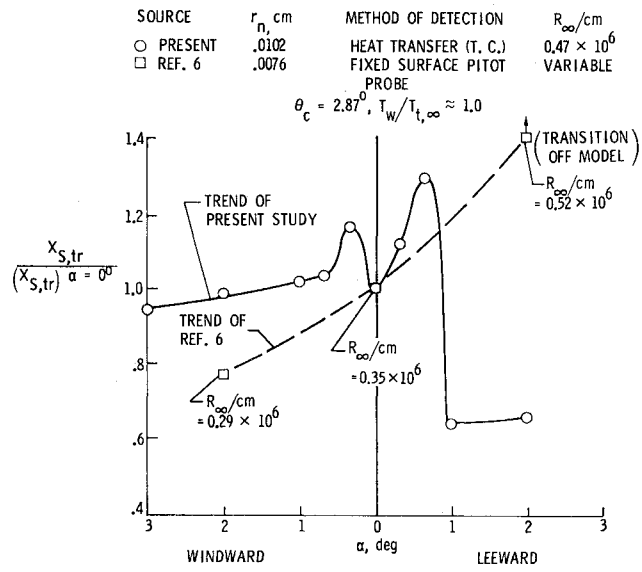

Fig. 2 Effect of angle of attack on cone boundary-layer transition.

Table 1 Comparison of cone (θ_c = 2.87°) transition Reynolds numbers for α = 0° and $T_w/T_{t,\infty} \approx$ 1.0

Source	r_n, cm	Method of detection	R_∞/cm	$(R_e)_{S,tr}$	M_e
Present	0.0102	Heat transfer (T.C.)	0.34 × 10^6	30.6 × 10^6	15.8
Ref. 6	0.0076	Fixed surface Pitot	0.35 × 10^6	45.2 × 10^6	15.8

large local Mach number and unit Reynolds number variation for small changes in angle of attack and instabilities in the crossflow from the windward to the leeward side. Transition behavior on the windward ray of the present study indicates transition "sticking" which was reported for cones only in Ref. 7 on a smooth sharp 6° half-angle cone at M_∞ = 10.

In Ref. 7, as in the present study, transition was determined from heat-transfer data which appears to be the preferable technique at hypersonic conditions. Preliminary angle-of-attack transition results obtained with the 152.4-cm-long cone tested in the Mach 20 leg of the Langley high Reynolds number helium tunnel, which has a 152.4-cm test section diameter, indicates the same transition behavior on the leeward and windward sides found in the 22-in. Mach 20 facility. This result rules out tunnel choking effects which may have been caused by positioning the 152.4-cm cone at angle of attack in the smaller 55.9-cm facility.

A comparison of the transition Reynolds number at α = 0° for the present study and that of Ref. 6 (identical cone, same test facility) at the same freestream conditions is given in Table 1 and indicates a transition Reynolds number about 30% less than reported in Ref. 6. In a previous hypersonic investigation[8] (M_e = 6.5, $T_w/T_{t,\infty} \approx$ 1.0) with a 10° half-angle wedge, transition determined from a surface Pitot probe occurred about 30% earlier than the transition location detected from heat-transfer data; the reverse of the effect noted in the present investigation at zero angle of attack. The discrepancy in transition Reynolds number level noted in Table 1 may be because of the inaccuracies associated with the surface Pitot probe technique for measuring transition at high hypersonic Mach numbers as compared to the heat-transfer technique. It should be mentioned, however, that at the conditions of the present investigation ($T_w/T_{t,\infty} \approx$ 1.0) the heat-transfer rates are low, and therefore liable to errors in absolute levels. However, the relative distribution of $\dot{q}$ along the cone (and thus transition) should indicate the correct trends.

In conclusion, boundary-layer transition at angles of attack in the range from 0° to 3° on a slender cone in a nominal Mach 20 flow was promoted on the leeward ray and essentially fixed on the windward ray, except at $\alpha < 1°$ where an apparent transition reversal occurs on both rays. These angle-of-attack transition results directly conflict with previously reported results with a cone of identical geometry tested in the same facility. The present transition results are believed to illustrate the correct trends as the results from the previous measurements were probably adversely influenced by the method of detecting transition.

References

[1] Stetson, K. F. and Rushton, G. H., "A Shock Tunnel Investigation of the Effects of Nose Bluntness, Angle of Attack and Boundary Layer Cooling on Boundary Layer Transition at a Mach Number of 5.5," AIAA Paper 66-495, Los Angeles, Calif., 1966.

[2] Fischer, M. C., "An Experimental Investigation of Boundary-Layer Transition on a 10° Half-Angle Cone at Mach 6.9," TN D-5766, April 1970, NASA.

[3] Stainback, P. C., "Effect of Unit Reynolds Number, Nose Bluntness, Angle of Attack, and Roughness on a 5° Half-Angle Cone at Mach 8," TN D-4961, 1969, NASA.

[4] Cleary, J. W., "Effects of Angle of Attack and Nose Bluntness on the Hypersonic Flow over Cones," AIAA Paper 66-414, Los Angeles, Calif., 1966.

[5] Nagamatsu, H. T., Graber, B. C., and Sheer, R. E., Jr., "Combined Effects of Roughness, Bluntness, and Angle of Attack on Hypersonic Boundary Layer Transition $M_1 = 8.5$ to 10.5," Rept. 65-C-011, Sept. 1965, G.E. Research and Development Center, Schenectady, N. Y.

[6] Maddalon, D. V. and Henderson, A., Jr., "Hypersonic Transition Studies on a Slender Cone at Small Angles of Attack," *AIAA Journal*, Vol. 6, No. 1, Jan. 1968, pp. 176–177.

[7] McCauley, W. D. Saydan, A. R., and Bueche, J. F., "Effect of Spherical Roughness on Hypersonic Boundary-Layer Transition," *AIAA Journal*, Vol. 4, No. 12, Dec. 1966, pp. 2142–2148.

[8] Wagner, R. D., Jr., Maddalon, D. V., and Weinstein, L. M., "Influence of Measured Freestream Disturbances on Hypersonic Boundary-Layer Transition," *AIAA Journal*, Vol. 8, No. 9, Sept. 1970, pp. 1664–1670.

Multiple Fourier Method for Plate Bending

NEVILLE I. ROBINSON*
Ohio State University, Columbus, Ohio

FOR the differential equation

$$\nabla^4 w = q/D \tag{1}$$

describing the bending of thin plates, a series solution may be found of the form,[1]

$$w = w_p + \sum_{j=1,2,3}^{\infty} a_j w_j \tag{2}$$

q is the transverse load, D the plate stiffness, w_p the particular solution of Eq. (1), w_j the homogeneous solutions forming a complete set, and a_j the constant coefficients determined by the boundary conditions,

$$G_1(w) = 0 = G_2(w) \tag{3}$$

The differential operators $G_{1,2}$ produce deflections, slopes, moments and shears depending on the type of boundary considered.

If the plate region is simply connected and star shaped, then any function defined along the boundary may be described uniquely by the angle θ from the datum of some appropriately selected origin. Hence the function at the boundary may be represented as a Fourier series in θ. Thus the terms $G_{1,2}(w_p)$ may be represented by Fourier series as also may each of the series terms $G_{1,2}(w_j)$. Equations (2) and (3) may then be transformed to

$$\sum_{j=1,2,3}^{\infty} a_j \left[\sum_{n=1,2,3}^{\infty} \epsilon_n (\alpha_{1,2jn} \cos(n-1)\theta + \beta_{1,2jn} \sin(n-1)\theta) \right] = -\sum_{n=1,2,3}^{\infty} \epsilon_n (\alpha_{1,2pn} \cos(n-1)\theta + \beta_{1,2pn} \sin(n-1)\theta) \tag{4a}$$

Table 1 Values of α for $w_{max} = \alpha q a^4/D$ for a uniformly, loaded simply supported rectangular plate

$b/a = 1$	0.0040636 (6)	0.0040632 (8)	0.0040624 (10)	0.0040624 (∞)
$b/a = 3$	0.012276 (8)	0.012236 (12)	0.012233 (16)	0.012233 (∞)
$b/a = 6$	0.013010 (24)			0.013010 (∞)

Received January 12, 1971.

* Postdoctoral Fellow, Department of Engineering Mechanics.

Table 2 Values of α for $w = \alpha q a^4/256D$ across the diagonal between corners of a uniformly loaded simply supported L-shaped plate

$16d$	0	1	3	5	7	9	11	13	15	16
Finite difference[4]	0	0.1	0.9	2.1	3.3	4.3	4.5	3.8	1.7	0
Integral equation[5]	...	0.1	0.9	2.1	3.4	4.5	4.8	4.2	2.5	...
Multiple Fourier	0	0.1	0.9	2.1	3.4	4.5	4.9	4.5	3.0	1.7

where the Fourier coefficients are given by

$$\begin{aligned}
\alpha_{1,2jn} &= \frac{2}{s}\int_0^s G_{1,2}(w_j)\cos\frac{2\pi}{s}(n-1)\theta d\theta \\
\beta_{1,2jn} &= \frac{2}{s}\int_0^s G_{1,2}(w_j)\sin\frac{2\pi}{s}(n-1)\theta d\theta \\
\alpha_{1,2pn} &= \frac{2}{s}\int_0^s G_{1,2}(w_p)\cos\frac{2\pi}{s}(n-1)\theta d\theta \\
\beta_{1,2pn} &= \frac{2}{s}\int_0^s G_{1,2}(w_p)\sin\frac{2\pi}{s}(n-1)\theta d\theta
\end{aligned} \tag{4b}$$

ϵ_n is a constant taking the value $\frac{1}{2}$ for $n = 1$, otherwise the value 1, and s is the periodicity $\leq 2\pi$. Equating coefficients in $\cos n\theta$ and $\sin n\theta$ in Eqs. (4a) the coefficients a_j may be determined from the matrix of linear equations

$$\begin{bmatrix} \epsilon_n \alpha_{1,2jn} \\ \epsilon_n \beta_{1,2jn} \end{bmatrix} \cdot [a_j] = -\begin{bmatrix} \epsilon_n \alpha_{1,2pn} \\ \epsilon_n \beta_{1,2pn} \end{bmatrix} \tag{5}$$

In practical numerical requirements of the solution of Eq. (5) it is necessary to truncate the series n at some value $2N$ and the series j at $4N$. The accuracy of solution will depend on the degree of convergence of the Fourier series for $2N$ terms. Smoothness, differentiability, discontinuities and periodicity of the functions are the well known governing factors of convergence. The rates of convergence of the Fourier series are related to the rate of convergence of the series in Eq. (2). A poor selection of series solutions in Eq. (2) and position of an origin(s) may produce very slow convergence. But, in any event, an increase in the number of terms will provide better solutions, except perhaps at points of discontinuity in boundary curvature ρ and transitions in boundary conditions and boundary loading.

For simplicity the Eqs. (4a, 4b, and 5) defining the Multiple Fourier method[2] were presented for a simply connected region. However, they are also valid for multiply connected regions, the α and β becoming summations of the form (4b) over the number of boundaries, and the number of terms in the Fourier series associated with one boundary possibly differing from those for another. Even though the method is simple the author has not been able to find published work for plate bending problems, although Pickett[3] intimates the use of a procedure essentially the same as the method described here but gives details only in the case of a classical single Fourier analysis for mixed polar and rectangular coordinate series.

Taking the $\Sigma^{2N} a_j w_j$ to be the polar series

$$\sum_{m=0,1,2}^{N-1} (A_m + B_m r^2) r^m \cos m\theta$$

for symmetrical uniformly loaded plates with an origin for radius r and angle θ in the central portion of the plate, the Multiple Fourier Method reduces to the classical single Fourier analysis for ring shaped plates[1] when boundary conditions are continuous.

The $2N(2N+1)$ integrations of Eqs. (4a) and (4b) have been performed numerically using Simpson's rule in the examples which follow, considerable savings in calculation being achieved by tabulating repetitive terms. In the case of continuous boundary conditions further saving is possible by